Biochemical Engineering Journal 186 (2022) 108592

Contents lists available at ScienceDirect

Biochemical Engineering Journal

journal homepage: www.elsevier.com/locate/bej

Physical characterization of oxygenic photogranules

Joseph G. Gikonyo *, Arfa Ansari, Chul Park, John Tobiason

Department of Civil and Environmental Engineering, University of Massachusetts Amherst, MA 01003, USA

ARTICLE INFO

Keywords:
Isopycnic centrifugation
Oxygenic photogranules
Hydrostatic
Sequencing batch reactors
Porosity
Permeability

ABSTRACT

This study investigated hydrodynamic properties of oxygenic photogranules (OPGs) generated in a sequencing batch reactor (SBR) treating wastewater without aeration and OPGs cultivated under hydrostatic conditions and used to seed an SBR reactor. Using isopycnic centrifugation the average density of OPGs was found to be 1037 kg/m3 and 1050 kg/m3 for the reactor OPGs and hydrostatic OPGs, respectively. The reactor OPGs had measured settling velocities in the range of 0.001–0.021 m/s while the hydrostatic OPGs had higher velocities, up to 0.07 m/s. The estimated porosity of reactor granules was 86 % while that of hydrostatic granules was 81 %. The porosity and settling velocities of reactor OPGs showed a general decrease with increasing granular size. In contrast, the porosity of the hydrostatic OPGs showed low correlations with granular size while their settling velocities decreased with increasing diameter (0.6–1.4 mm). These physical parameters reflect OPGs amenability to rapid solids separation during wastewater treatment. Moreover, the high porosity and low permeability reflect the microbial mobility with increasing size to optimize functionality especially related to motile filamentous cyanobacteria. Strategies utilizing size based bioreactor operations for different treatment objectives and optimized agitation minimizing energy use towards environmental stewardship in treatment can also be achieved.

1. Introduction

The application of photogranular technology for wastewater treatment is gaining widespread interest [1–3]. The utility of each granular aggregate as an autonomous reactor in which biotransformation ensues gives many operational benefits compared to canonical wastewater treatment systems [2]. Compared to other granules, photogranules have the added advantage of self-aerating potential negating the need for energy-intensive aeration [1,4]. Moreover, microalgal-bacterial aggregates have been reported to have superior nutrient removal capability with adequate irradiance compared to aerobic sludge granules [2].

Oxygenic photogranules (OPGs) have recently been investigated and characterized for aeration-free wastewater treatment [4–8]. These photogranules have microbial consortia consisting of phototrophic organisms, predominantly motile filamentous cyanobacteria, and algae, on their outer surfaces while heterotrophic, nitrifying, and denitrifying bacteria colonize their interior zones [5,7,9]. An oxygen gradient exists into the granular core, due to aerobic conditions at the exterior granular surface and anaerobic or anoxic cores [5,10]. This stratification could result in a spatial functional variation similar to that present in biofilms [11,12], and is enhanced by motility of cyanobacteria in response to environment and substrate fluxes [13,14].

The generation of oxygen in OPG reactor operations relies on agitation to maintain the biomass in suspension [1], and to continually expose photosynthetic consortia to light substrate [4]. The operational pressures including shear [15], light [16,17], and substrate concentrations [18], affect granular size development and subsequently their density and function [2,5]. Moreover, the suspension rheology continually changes in the shear force field of the bulk fluid and with particle-particle interactions [19].

The design of an effective OPG wastewater treatment process, requires an understanding of the physical characteristics of the granules, including their size, density, permeability, and porosity, which affect their hydrodynamic behavior and function; this study presents the first such physical characterization of OPGs. The physical properties including density, settling velocity were investigated, and applied to model the porosity, and permeability of reactor OPGs in varying size groups as well as OPGs cultivated under hydrostatic conditions and used to seed OPG reactors. Characterizing these physical properties can facilitate prediction of OPG movement within the reactor to optimize their interactions with light. Further this can be used to optimize mixing operations for operational sustainability.

* Corresponding author.
E-mail address: jgikonyo@umass.edu (J.G. Gikonyo).

https://doi.org/10.1016/j.bej.2022.108592
Received 14 April 2022; Received in revised form 23 July 2022; Accepted 15 August 2022
Available online 17 August 2022

2. Materials and methods

2.1. Generation of OPGs

The reactor OPG biomass was generated in a sequencing batch reactor (SBR) without mechanical aeration treating wastewater (primary effluent) from the local wastewater treatment plant. The glass reactor had an internal diameter of 22.7 cm, a total height of 24 cm, and was operated at an 8 L working volume. The reactor was operated in sequential light (first)-dark photoperiods each 3-hours long with a 180 μmol m^{-1} s^{-1} light intensity for each treatment cycle, giving 4 treatment cycles per day and a 1-day hydraulic retention time (HRT). The feed and decant durations were maintained below 0.025 of the total cycle time. At the onset 20 OPG seed granules generated under hydrostatic conditions as reported in prior work [1,20], were inoculated into the reactor. Briefly, 20 mL of activated sludge harvested from the local wastewater utility was incubated in closed vials under 150 μmol m^{-1} s^{-1} light for 30 days to generate hydrostatic seed granules.

Influent wastewater had a chemical oxygen demand (COD) of between 65 mg/L and 200 mg/L (average 117 ± 45 mg/L), Ammonia concentrations were 15 ± 6 mg/L and Phosphorous 2.8 ± 0.5 mg/L. Effluent COD concentrations were between 27 and 52 mg/L, with average removal of 70 % while Nitrogen and phosphorous had 80 % and 35 % removals, respectively.

2.2. Biomass characterization

Reactor granules were collected and examined on day 95. OPGs generated by hydrostatic incubation of an activated sludge inoculum from the same wastewater treatment plant were also examined. The harvested reactor OPGs (hereafter denoted as SBR OPGs) and hydrostatically formed OPGs were classified into assorted sizes using sieve analysis (ATSM E-11, ISO 565). The wet sieving method [5], involved sequentially passing the SBR OPGs through sieves with openings of 0.10 mm, 0.20 mm, 0.30 mm, 0.50 mm, 0.71 mm 1.0 mm,1.70 mm and 3.36 mm. Granules retained between intervening sieve sizes were resuspended in 0.45 μm filtered effluent water and classified as size classes 1–7, respectively, for which subsequent characterization was conducted on equal volumes of well mixed biomass samples.

Biomass concentrations were evaluated for volatile (VS) and total solids (TS) fractions according to Standard Methods (2540D) [21]. The photosynthetic chlorophyll pigments were extracted and quantified following Standard Methods 10,200 H [21]. Additionally, phycobilin, accessory pigments of cyanobacteria, were extracted and quantified as described by Abouhend et al. (2020) [5] with some modifications. Specifically, all centrifugation unit operations were undertaken at 12, 000 rpm while supernatant absorbances were measured using a spectrophotometer (Genesis 10 S UV–VIS) at 280 nm, 495 nm, 566 nm (for phycoerythrin), 620 nm (for phycocyanin), 652 nm (for allophycocyanin), 675 nm, and 750 nm wavelengths. The 750 nm wavelength was used to correct for sample turbidity [22], while the 495 nm was used to quantify chlorophyll *a* interference [23]. The Bennett and Bogorad equations were used to quantify phycobilin concentrations [24].

2.3. Settling of OPGs

For the free particle settling test, a vertically mounted transparent plastic cylinder 2.50 m in height and 0.05 m in diameter filled with reactor liquid effluent pre-filtered through 0.70 μm membrane filters was used. Markers were placed at 0.25 m from the cylinder top and capped bottom denoting 2 m and 0 m distances, respectively. Intermediate distances of 0.50 m were also marked out with an accuracy of ± 0.005 m. Before each free settling test, granules from the various size clusters was photographed for further image analysis (Image Pro v.10, Media cybernetics) to acquire particle size parameters. The granule shape was characterized using a circularity parameter (Image Pro v.10, Media cybernetics) being the deviation from a perfect circle. Circularity was applied as a proxy for particle sphericity. The granules were introduced, one by one at the top of the column, with video recording tracking the movement of granules in the column. The videos were split into frames (VLC-videolan.org) and processed to collect time lapse details of granules passing each marker between 1.50 m and 0.50 m with an accuracy of ± 0.05 s. Average settling velocities were calculated based on distance travelled and elapsed time for each granule and matched to its size parameters.

2.4. Density measurement

The estimation of the density of OPGs was undertaken using isopycnic centrifugation. A stock isotonic solution was prepared by diluting a Percoll® Plus commercial product with 1.5 M NaCl at 9:1 parts (v/v). The stock solution was further diluted with 0.15 M NaCl to achieve 6 discrete density concentrations in the range of 1.0–1.13 g/mL. 25 mL of each density concentration solution was pipetted into separate 30 mL centrifuge tubes. A 50 μL volume of density marker beads (Cospheric™) in the target density range was then added prior to centrifuging (Sorvall™ RC 5 C plus) at 10,000 rpm, 12,000 rpm, 13,000 rpm, 15,000 rpm and 17,000 rpm each for 15 min. The corresponding relative centrifugal forces (RCF) with a fixed angle rotor (Sorvall SA600) of 34° were 14,476, 20,846, 24,465, 32,572 and 41,837, respectively. Additional stock dilutions were also centrifuged for 60 min and 90 min at 13,000 rpm, and for 30 min and 45 min at 17,000 rpm. Calibration curves were prepared, and the resulting density values were confirmed by correlation with refractive index measured using a digital refractometer (Hanna Instruments). The height of each marker band from the tube bottom was plotted against the density of each band as indicated in supplemental information. The experiment was conducted at a temperature of 23 ± 1 °C. Optimal stock solution dilution (40 %) and centrifugation conditions (13,000 rpm, 90 min) were selected based on the linearity of this density-depth relation and used for estimating the density of the OPGs.

Density estimations were undertaken for OPGs harvested from the SBR and sorted by sieve analysis into assorted sizes. Centrifuge tubes with 40 % solution of the standard isotonic Percoll (SIP) were centrifuged at 13,000 rpm for 90 min to create continuous density gradients. Multiple dewatered samples ($5 < n < 30$) of each granule size cluster were introduced in separate centrifuge tubes and centrifuged for 30 min at 500 rpm (RCF-36). A separate tube with calibration marker beads was included with each test. Granules of the same size class settled in a density layer within a 0.3 cm margin. The location of both granules and marker beads was measured as the mid-point of each layer from the bottom of the centrifuge tubes to the nearest 0.1 cm. Hydrostatically formed OPGs collected from incubation vials and sized using image analysis were similarly characterized for density but with 17,000 rpm centrifugation for 30 min. The determined velocities and temperature (23 °C) adjusted water density (997.53 Kg/m^3) were also applied for Stokes (unmodified) density estimations.

2.5. Analytical procedure

The free settling test of discrete particles in an infinite fluid medium is described by Stokesian laws that balance the buoyant and drag forces against the particle weight [25]. While this estimation is highly accurate for solid particles, velocity amendment by fluid flow through porous and highly permeable media can underestimate density measurements [26]. This velocity relation when modified to account for particle porosity (*e*) and permeability can be expressed as follows, [26]:

$$V^2 = \frac{4gd_{opg}\left(\rho_{opg} - \rho_l\right)(1-e)}{3\rho_l \Omega C_D} \quad (1)$$

where g is the gravitational force (m/s^2), e the porosity, d_{opg} is particle

diameter (m), and C_D is the drag coefficient. Image analysis was used to determine diameter of OPGs while the free settling test was used to evaluate the terminal velocity (V). The parameters ρ_{opg} and ρ_l are the densities of the OPGs and the liquid, respectively. The flow factor (Ω) describes the flow resistance through the granule body and can be calculated for a porous sphere as below [26,27];

$$\Omega = \frac{2\beta^2[1 - tan \quad \beta/\beta]}{2\beta^2 + 3[1 - tan \quad \beta/\beta]} \tag{2}$$

Where β is a normalized particle diameter given by (Eq. 3),

$$\beta = d_{opg} \Big/ 2\sqrt{k} \tag{3}$$

Where k is the permeability (m^2) estimated using the Brinkman model [28];

$$k = \frac{d_{opg}^2}{72}\left(3 + \frac{4}{1-e} - 3\sqrt{\left(\frac{8}{1-e} - 3\right)}\right) \tag{4}$$

Finally, the drag coefficient (C_D) was estimated using the Masliyah and Polikar estimation for permeable porous spheres [28].

$$C_D = \frac{24\Omega}{Re}\left(1 - YRe^{(X-Zw)}\right) \tag{5}$$

Where $= log_{10}Re$, and the Reynolds number, $Re = \rho_{opg} v d_p/\mu$ with μ being the fluid viscosity. The coefficients Y, X, and Z are 0.1315, 0.82, and 0.05, respectively for 0.1 <Re≤ 7 and 0.0853, 1.093, and 0.105 for 7 <Re< 120. The solid fraction 1-*e* was calculated as per (Eq. 1) by minimizing estimated values of porosity (*e*) using OpenSolver 2.9.4. (Opensolver.org) [29]. The Pearson correlation coefficient was used to characterize the association between variables.

3. Results and discussion

3.1. Settling velocity

The average settling velocity of SBR OPGs (Fig. 1) (n = 89) was 0.0086 m/s (range:

0.0031–0.022 m/s) with a diameter range of 0.30–2.70 mm (Fig. 2). This corresponds to Reynolds numbers ranging from 1.3 to 40. In agreement with Stokes law, a general increase of settling velocity with increasing particle size was observed for reactor granules. Abouhend et al., 2020 [5], reported a zone settling velocity for OPGs in the range of

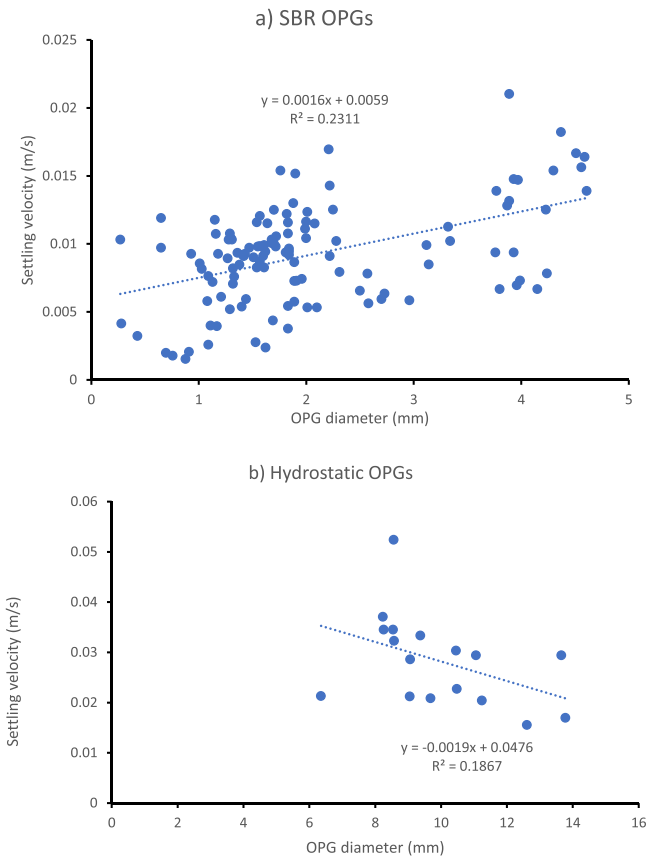

Fig. 2. Settling velocity of individual OPGs. a) Sequencing batch reactor OPGs, b) hydrostatically-formed OPGs. The dotted line is a linear regression fit of the data with equation presented on the plot. Error bars show the standard error of the measured values.

0.0008–0.022 m/s for granular cohorts of comparable size classes. The average velocity of 0.0086 m/s closely matches the reported zone settling velocity (ZSV) for OPG granules of 0.50–1.00 mm diameter as 0.0067 ± 0.0014 m/s. The authors in this case reported a ZSV for mixed biomass as 0.004 ± 0.001 m/s. Particle-particle and particle-fluid interference alters the settling behaviour and is a function of Re and particle spacing [30,31]. The interference and higher effective diameter

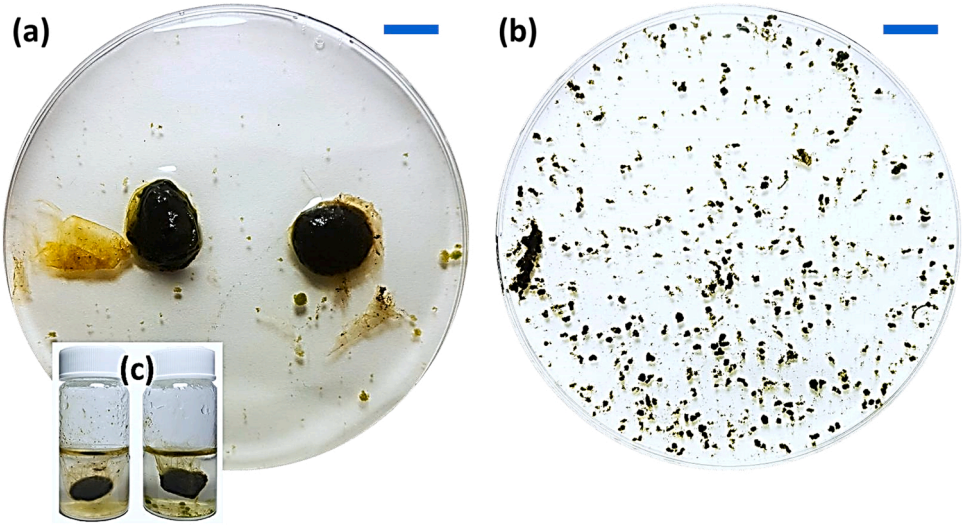

Fig. 1. Sample oxygenic photogranules. a) Hydrostatic OPGs, b) Sequencing batch reactor OPGs, c) Hydrostatic incubation 20 mL vials. The scale bars are 1 cm for the petri dish images while the vials inset is not to scale.

(weight) of more particles could explain the slight variations between reported ZSV and settling velocity experimental results.

In contrast, a general decline in settling velocity with increasing size for hydrostatic granules (Fig. 2) was observed. The average settling velocity of hydrostatically-formed OPGs (Fig. 1) (n = 17) was 0.027 m/s (range: 0.01–0.05 m/s) (Fig. 2). Moreover, the larger sizes of hydrostatic OPGs with diameters in the range of 6.00–14.00 mm resulted in higher Reynolds numbers of 151–498. The amendment of the wake (flow separation) by internal flow permeation lowers particle drag, increasing settling velocities. However, at Re> 100 porous particles experience higher drag due to frictional drag, reduced pressure drag or altered wake region decreasing velocities [32]. Additionally, while SBR OPGs had an average circularity of 0.70, that of hydrostatic OPGs was 0.56. Weak correlation was observed between particle sizes and their circularity with correlation coefficient of 12 % for both SBR and hydrostatic granules. Hydrostatic granules with manifest rougher edges could experience higher frictional resistances lowering settling velocity as size increases. Furthermore, the velocity amendment by granule surface characteristics is reflected in the weak OPG diameter-Settling velocity correlations (Fig. 2) and may result in uncertainty of other derived parameters using the stokes model.

Physical and hydrodynamic properties of granules impact their effectiveness in wastewater treatment applications. Primarily, the lure of a granular bioreactors is better solids settleability, which improves separation from the bulk liquid as compared to activated sludge [1,3]. Better settleability (Fig. 2) of granules enables higher biomass retention within the reactor presenting opportunities for wastewater treatment process intensification reducing the treatment environmental footprint. In addition, photogranules have self-aerating potential in contrast to activated sludge or aerobic sludge granular systems which rely on energy intensive mechanical aeration [1,3,20]. In reactor operation, OPG settling velocity profiles can be amended via entrapment in flocculent settling biomass. The variable settling profiles of OPG biomass can also be utilized for operational management schemes to achieve target treatment objectives. Granules functionality have been linked to size variations impacting distribution of microbial communities [5].

3.2. Estimation of OPG density

Higher centrifugation speeds and time resulted in steeper isopycnic gradient curves while a higher dilution of the SIP enhanced the linearity of calibration curves. The linear sections of the calibration curves (Fig. 3) ware used to estimate particle density. SBR OPGs were evaluated using an optimal linear model achieved with 13,000 rpm, 90 min, and 40 % dilution conditions. On the other hand, hydrostatic OPGs were evaluated using a calibration curve developed with 17,000 rpm, 30 min, and 40 % dilution due to their higher settled profiles. The hydrostatic calibration curve was split into two zones, below and above 2 cm from the centrifuge tube bottom (Fig. 3).

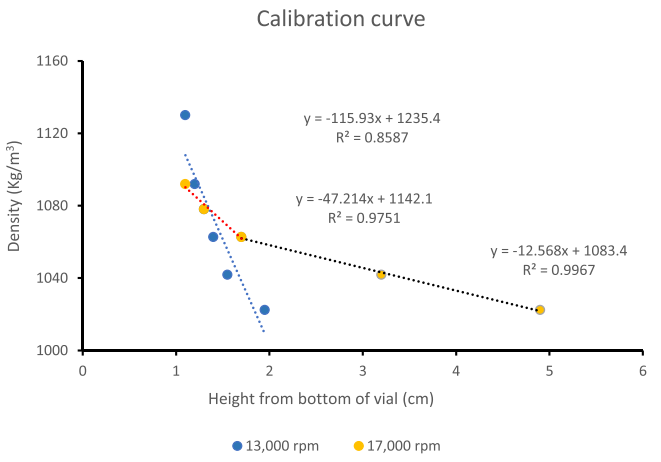

Fig. 3. Density calibration curves from isopycnic centrifugation of density marker beads. The linear model fits for the data are shown for (○) SBR OPGs (1) at 13,000 rpm, (Δ) hydrostatic OPGs with < 2 cm height and 17,000 rpm (2), and (◊) hydrostatic OPGs at > 2 cm height and 17,000 rpm (3).

For the SBR OPGs examined, the average density was 1037 kg/m^3 (std. dev 22) (Fig. 4) with a Pearson correlation coefficient of − 0.62 between size and density. The average densities were 1042 kg/m^3 (std. dev 3.3) for granules 0.10–0.50 mm in size, and 1044 kg/m^3 (std. dev 8.2) for sizes between 0.60 and 1.00 mm. These densities were higher than those of granules with dopg> 1.00 mm in size (mean: 1021 kg/m^3, std. dev 8.2). For hydrostatically-formed OPGs, three density estimations were conducted. Firstly, granules that settled lower than 2 cm from the centrifuge tube bottom had an estimated average density of 1056 kg/m^3 (std.dev 7.1). Secondly, the density of granules that settled at higher isopycnic gradients had an estimated average density of 1050 kg/m^3 with a range of 1043–1057 kg/m^3 and a correlation coefficient of 0.42 with the granule size. Finally, the density of hydrostatically-formed OPGs was estimated using Stokes law (unmodified) and their settling velocities. This estimation resulted in an average density of 998 kg/m^3 (range: 997–999 kg/m^3). The departure of the experimental density determinations from the solid sphere density assumption implicit in Stokesian estimations can be attributed to non-sphericity of OPG granules, their porosity amending drag forces, and experimental errors.

Agitation via aeration and mixers is used to distribute fluxes in activated sludge in addition to inducing shear selection pressure for aerated granular matrices. Photogranules likewise require some degree of mechanical suspension to enhance interaction with light and for granulation [18]. The intensity of this agitation for suspension is reliant on granule density properties. The closely commingled morphology comprising various microbes embedded in an extracellular polymeric matrix [20], alters OPG density relative to the bulk fluid and changes with granular growth [33]. The density of sampled SBR OPGs was found to be in the range of 1015 kg/m^3 to 1061 kg/m^3 (Fig. 4). This estimated maximum density of OPGs was lower than that reported for activated sludge biomass 1038–1070 kg/m^3 [25,34] and higher than that of aerobic granules 1037–1049 kg/m^3 [26]. The higher density of activated sludge can be attributed to experimental differences between adopted stokesian (modified) estimation [25,34], and isopycnic estimation applied herein.

The proximity of OPG densities to that of water eases their suspension in liquid by agitation while their higher density relative to that of water is amenable to gravity separation. Granular morphologies are dominated by discrete settling mechanics [35]. SBR OPGs had lower settling velocities (0.003–0.020 m/s) than those for

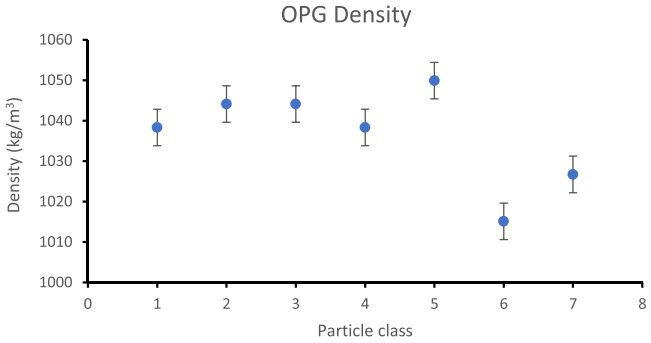

Fig. 4. The density of different sized OPGs. (a) SBR OPGs for each size class 1 (0.1–0.2 mm),2 (0.2–0.3 mm),3 (0.3–0.5 mm),4 (0.5–0.71 mm), 5 (0.71–1.0 mm),6 (1–1.7 mm), 7 (1.73.36 mm) obtained via sieve analysis (ATSM E-11 for size>2.36 and ISO 565 for all smaller sizes) with (n > 10). (b) Individual hydrostatic OPGs. Error bars show the standard error of estimated values.

hydrostatically-formed OPGs (0.020–0.050 m/s) (Fig. 2) and aerobic sludge granules (0.02–0.07 m/s) [33]. Abouhend et al.,2018 reported comparable settling velocities of 26–91 m/h for individual photo-granules of 1–4.5 mm diameter [1].

3.3. Determination of porosity and permeability

The measured free settling velocities and estimated particle class densities were substituted in Eq. (1) to estimate the porosities (e) of individual granules. SBR OPGs had estimated average porosity of 86 % (Fig. 5a) while that of hydrostatic OPGs was on average 81 % (Fig. 5b). The porosity of SBR OPGs generally decreased with size while that of hydrostatic OPGs remained constant with increasing size. Reactor granules with an outlier characteristic porosity of 81 % comparable to that of hydrostatic granules was observed. Eliminating the outliers improved the model fit by 50 % to a correlation coefficient of 0.47. The estimated permeability (Eq. 4) did not have any discernible trends with particle size for reactor granules with a mean of 1.35×10^{-10} m^2 (Fig. 6a). Most reactor granules > 2.5 mm in diameter had permeabilities comparable to hydrostatic OPGs. The permeability of hydrostatic granules increased with size with a mean of 2.68×10^{-16} m^2 (Fig. 6b) and a coefficient correlation of 0.99.

The range of porosities for SBR OPGs (81–97 %) (Fig. 5) was comparable to that reported for aerobic granule sludge (65–90 %) but with higher limit values. Hydrostatically-formed OPGs, on the other hand, had porosities of 81–83 % (Fig. 5) and lower permeabilities (Fig. 6). Hydrostatic OPGs have been reported to have an extensive network of polysaccharide-based EPS, which transforms from slime to tubular structure with maturation [20]. Secretion of these EPS and other types of EPS can alter the physical properties of microbial structures including density and porosity [36]. The photo-taxis of motile filamentous bacteria with increasing granular size to outer layers is aided by these extensive hollow sheaths enmeshed in a honeycomb structure (Fig. S1), which could be responsible for the increasing hydrostatic OPGs permeability with size and also reflected in their size-velocity inverse relation (Fig. 2). Similarly, the plugging of pores by EPS gel matrix was reported to reduce the porosity and permeability in aerobic granules

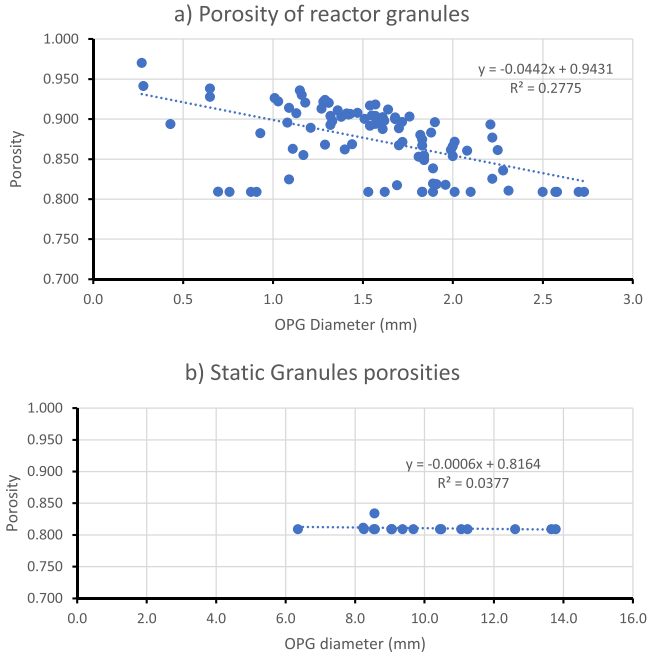

Fig. 5. Estimated porosities of different OPG sizes. (a) reactor OPGs. (b) hydrostatic OPGs. Dotted lines show the corresponding linear regression fit to the data with respective models and fit coefficients indicated on plot.

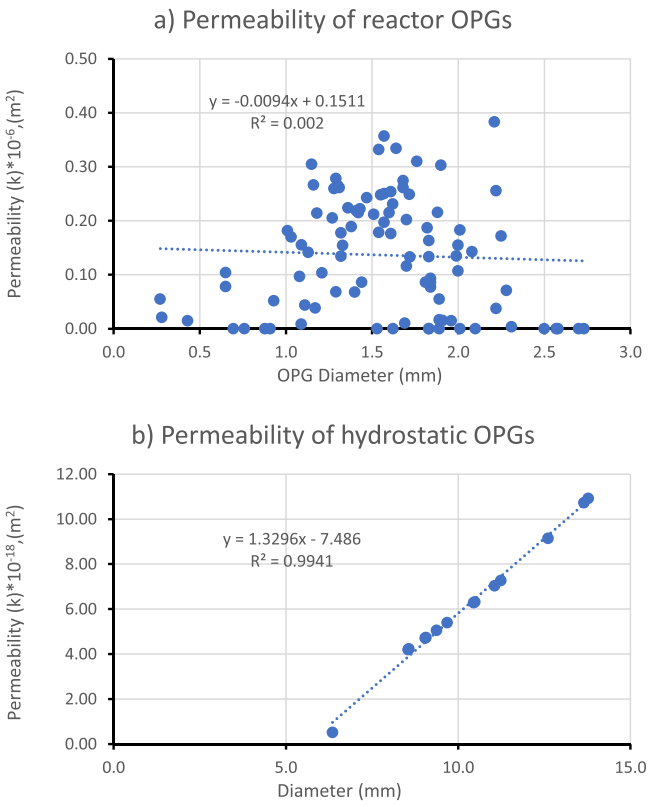

Fig. 6. Estimated permeability for different OPG sizes. (a) Reactor OPGs. (b) hydrostatic OPGs. Dotted lines show the corresponding exponential and linear regression fits, respectively, to the data with models indicated. The permeability scales for reactor granules is 10^{-6} while that of hydrostatic granules is 10^{-18}.

from reactors [33]. In contrast, the higher porosity and permeability in SBR OPGs suggests shear influence on granular growth by attrition resulting in more compact structures [15]. As reactor granule increased in size their permeabilities decreased significantly comparably to hydrostatic granules suggesting inhibited substrate transfers at their centers.

Likewise, agitation provides suspension of granules for OPG interaction with a light source within the reactor [18]. The resulting particle-particle interactions and OPG dynamic behavior relative to the bulk fluid is influenced by their physical characteristics. Isopycnic density measurements lends to easy estimation of hydrodynamic characteristics despite assumptions made in the estimation of porosity using Eq. (1) [25]. The estimated permeability and porosity suggests the existence of substrate advective and diffusive mass transfer into the granular structure dependent on application [1,18,26]. Dispersive propagation of bulk fluid velocities beyond the conventional bulk advection-diffusion boundary layer used in modelling granular systems could significantly influence substrate conveyance in shear based OPG reactor systems [37,38]. Localized occupation by microbial communities in layered niches to optimize functionality within the granular matrix can be utilized to achieve different wastewater treatment objectives. For example, smaller granules with high porosity and light penetration can be utilized for aeration purposes, and nitrification, while larger granules with less permeability and potential anaerobic zones for bio-reduction [5].

3.4. Phototrophic characterization of granular biomass

Granular solids and pigment concentrations were characterized for the SBR OPGs. The ratio of volatile to total biomass solids was, on

average, 0.86 (std. dev=0.006), with granules of size class 4 (0.50–0.71 mm), and 5 (0.71–1.00 mm), having the highest biomass solids concentrations (Fig. 7). The VS/TS ratios ware comparable to values reported elsewhere for OPGs [1,8,18].

The concentration of chlorophyll pigments had an increasing trend with a peak in class 4, but granules of size class 7 (1.70–3.36 mm) had the highest chlorophyll pigment (Fig. 8a), and phycobilin concentrations (Fig. 8b). Phycobilin, an accessory pigment, in tandem with chlorophyll *a* pigment, constitute the light harvesting complex of Cyanobacteria. Motile filamentous Cyanobacteria of subsection III [39],have been reported as essential for the formation of OPGs [20,40]. The trend of chlorophyll *b* concentration followed that of chlorophyll *a* (Fig. 8a). While no general relation between pigments concentration and size was observed, an initial increasing trend of concentration up to size class 4 (0.50–0.71 mm) ensued. Chlorophyll *b* and chlorophyll *a* pigments are associated with algae light harvesting moiety [41]. An increase of chlorophyll *c* (Fig. 8a), an accessory light-harvesting pigment associated with diatoms [4], with increasing size of granules was observed.

Microbes in OPGs form functionally differentiated layers varying with granular size [5]. Congruent with previous reports, biomass concentrations (Fig. 7) were highest in the 0.50–1.00 mm size class [5]. Moreover, the concentration of pigments were also high in this size class (Fig. 8). Layered structural development a corollary of microbial communities' distribution with granule size contributes to structural non-homogeneity and consequently variable substrate transport. Microalgae have both chlorophylls *a* and *b* in their light-harvesting moiety while cyanobacteria have both chlorophyll *a* and phycobilin accessory pigments [4]. These pigments harness light energy for photosynthesis generating oxygen. Oxygen liberated from the photosynthetic oxidation of water is transferred into the granular core or out into the bulk fluid while carbon dioxide from bacterial respiration transports towards the granular surface [3,4]. The flow of bulk fluid through the permeable OPG structure transfers substrates dissolved in wastewater into granules. In contrast, the transfer of substrates and mechanically provisioned oxygen in aerobic granules is unidirectional into the granule [42].

In this study physical properties of oxygenic photogranules used for wastewater treatment were investigated. The density determined can be applied in dynamic particle and fluid transport models detailing the movement of OPGs relative to each other and the bulk fluid. These models provide correlations of agitation speeds to rates of granular transition within bioreactors and can be used to predict frequency of exposure to light zones. Understanding light exposure is essential in optimizing the interaction of OPGs with light within reactors to maintain treatment effectiveness and lowering bioprocess energy consumption. OPGs were found to have high porosity and significant permeability which can impact their density. Each granule can be considered a singular bioreactor, and the consideration of porosity and permeability influences on advective-dispersion transport could improve intra-granule transport models. The better settleability of OPGs despite comparable density to activated sludge is due to discrete settling mechanics for granules in contrast to flocculent settling for activated sludge.

4. Concluding remarks

- The settling velocity of OPGs increases with size in shear environments with a mean velocity of 0.0086 m/s. Larger OPGs grown in hydrostatic environments had a converse size-velocity relation with mean settling velocity of 0.0027 m/s.
- The average density of OPG granules was found to be 1037 and 1050 kg/m^3 for reactor and hydrostatic granules respectively.
- Modelled OPGs porosity was greater than 80 % for the granules evaluated while the permeabilities were 1.35×10^{-10} m^2 and 2.68×10^{-16} m^2 for reactor and hydrostatic granules respectively.

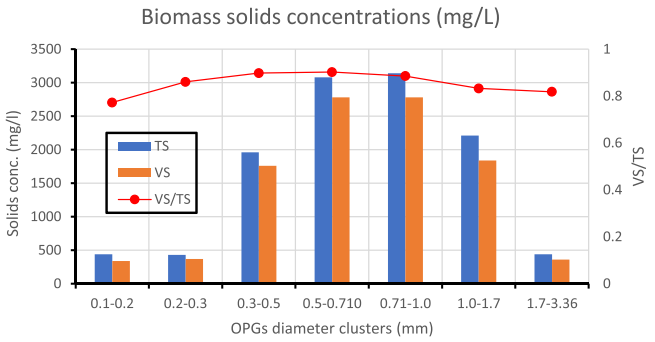

Fig. 7. The biomass fraction concentrations for SBR OPGs of distinct size classes. The x-axis values are the OPG class sizes obtained via wet sieve separation method. Error bars are standard errors of duplicate samples. TS and VS are the total and volatile biomass fractions, respectively.

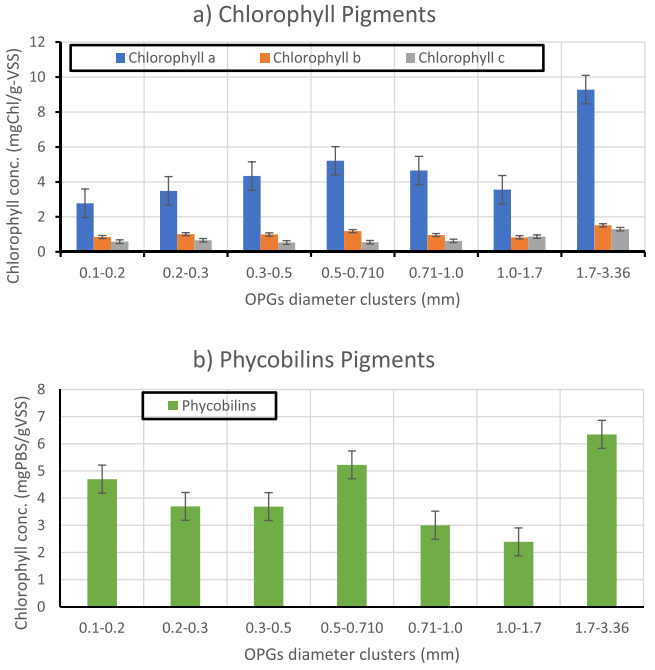

Fig. 8. Photosynthetic pigments concentration in SBR OPGs of distinct size classes with standard error bars shown. Values shown are concentrations normalized to volatile biomass concentrations (g/l). The x-axis shows the diameter range of each granule size class (mm).

Declaration of Competing Interest

The authors declare the following financial interests/personal relationships which may be considered as potential competing interests: Chul Park reports financial support was provided by National Science Foundation. Joseph Gitau has patent pending to University of Massachusetts. Chul Park has patent issued to University of Massachusetts.

Acknowledgements

The authors greatly thank Coretta K. Nyambura and Andrew Keyser for their assistance in the analysis. This work was supported by the National Science Foundation [IIP1919091].

Appendix A. Supporting information

Supplementary data associated with this article can be found in the online version at doi:10.1016/j.bej.2022.108592.

References

[1] A.S. Abouhend, A. McNair, W.C. Kuo-Dahab, C. Watt, C.S. Butler, K. Milferstedt, J. Hamelin, J. Seo, G.J. Gikonyo, K.M. El-Moselhy, C. Park, The oxygenic photogranule process for aeration-free wastewater treatment, Environ. Sci. Technol. 52 (2018) 3503–3511, https://doi.org/10.1021/acs.est.8b00403.

[2] Y.-J. Lee, Z. Lei, Microalgal-bacterial aggregates for wastewater treatment: a mini-review, Bioresour. Technol. Rep. (2019), 100199, https://doi.org/10.1016/j.biteb.2019.100199.

[3] G. Quijano, J.S. Arcila, G. Buitrón, Microalgal-bacterial aggregates: applications and perspectives for wastewater treatment, Biotechnol. Adv. 35 (2017) 772–781, https://doi.org/10.1016/j.biotechadv.2017.07.003.

[4] J.G. Gikonyo, A. Keyser, J. Tobiason, J. Jeong, C. Park, In vivo evaluation of oxygenic photogranules' photosynthetic capacity by pulse amplitude modulation and phototrophic–irradiance curves, ACS EST Eng. (2021), https://doi.org/10.1021/acsestengg.0c00221.

[5] A.S. Abouhend, K. Milferstedt, J. Hamelin, A.A. Ansari, C. Butler, B.I. Carbajal-González, C. Park, Growth progression of oxygenic photogranules and its impact on bioactivity for aeration-free wastewater treatment, Environ. Sci. Technol. 54 (2020) 486–496, https://doi.org/10.1021/acs.est.9b04745.

[6] C. Park, S. (deceased) Dolan, Algal-sludge granule for wastewater treatment and bioenergy feedstock generation, US 10,189,732 B2, 2019. ⟨https://www.researchgate.net/publication/330712356_Patent_Algal_Sludge_Granule_OPG_Jan_2019/related⟩ (Accessed 1 February 2019).

[7] K. Milferstedt, J. Hamelin, C. Park, J. Jung, Y. Hwang, S.-K. Cho, K.-W. Jung, D.-H. Kim, Biogranules applied in environmental engineering, Int. J. Hydrog. Energy 42 (2017) 27801–27811, https://doi.org/10.1016/j.ijhydene.2017.07.176.

[8] A.A. Ansari, A.S. Abouhend, C. Park, Effects of seeding density on photogranulation and the start-up of the oxygenic photogranule process for aeration-free wastewater treatment, Algal Res. 40 (2019), 101495, https://doi.org/10.1016/j.algal.2019.101495.

[9] K. Stauch-White, V.N. Srinivasan, W. Camilla Kuo-Dahab, C. Park, C.S. Butler, The role of inorganic nitrogen in successful formation of granular biofilms for wastewater treatment that support cyanobacteria and bacteria, AMB Express 7 (2017), https://doi.org/10.1186/s13568-017-0444-8.

[10] M. Hann, Factors Impact Cultiv., Struct., Oxyg. Profiles Oxyg. Photo Aeration-Free Wastewater Treat. (2018), https://doi.org/10.7275/3GH4-EN49.

[11] Z. Lewandowski, J.P. Boltz, Biofilms in Water and Wastewater Treatment, in: Treatise Water Sci, Elsevier, 2011, pp. 529–570, https://doi.org/10.1016/B978-0-444-53199-5.00095-6.

[12] D.H. Limoli, C.J. Jones, D.J. Wozniak, Bacterial extracellular polysaccharides in biofilm formation and function, Microbiol. Spectr. 3 (2015), https://doi.org/10.1128/microbiolspec.MB-0011-2014.

[13] R.W. Castenholz, F. Garcia-Pichel, Cyanobacterial responses to UV radiation, in: B. A. Whitton (Ed.), Ecol. Cyanobacteria II, Springer, Netherlands, Dordrecht, 2012, pp. 481–499, https://doi.org/10.1007/978-94-007-3855-3_19.

[14] V. Donkor, D.-P. Häder, Effects of solar and ultraviolet radiation on motility, photomovement and pigmentation in filamentous, gliding cyanobacteria, FEMS Microbiol. Lett. 86 (1991) 159–168, https://doi.org/10.1016/0378-1097(91)90661-S.

[15] Y. Liu, J.-H. Tay, The essential role of hydrodynamic shear force in the formation of biofilm and granular sludge, Water Res. 36 (2002) 1653–1665. ⟨http://www.sciencedirect.com/science/article/pii/S0043135401003797⟩ (Accessed 21 April 2017).

[16] P. Dechatiwongse, S. Srisamai, G. Maitland, K. Hellgardt, Effects of light and temperature on the photoautotrophic growth and photoinhibition of nitrogen-fixing cyanobacterium Cyanothece sp. ATCC 51142, Algal Res 5 (2014) 103–111, https://doi.org/10.1016/j.algal.2014.06.004.

[17] K. Lee, C.-G. Lee, Effect of light/dark cycles on wastewater treatments by microalgae, Biotechnol. Bioprocess Eng. 6 (2001) 194–199, https://doi.org/10.1007/BF02932550.

[18] J.G. Gikonyo, A.A. Ansari, A.S. Abouhend, J.E. Tobiason, C. Park, Hydrodynamic granulation of oxygenic photogranules, Environ. Sci. Water Res. Technol. 7 (2021) 427–440, https://doi.org/10.1039/D0EW00957A.

[19] C. Datt, G.J. Elfring, Dynamics and rheology of particles in shear-thinning fluids, J. Non-Newton. Fluid Mech. 262 (2018) 107–114, https://doi.org/10.1016/j.jnnfm.2018.03.016.

[20] W.C. Kuo-Dahab, K. Stauch-White, C.S. Butler, G.J. Gikonyo, B. Carbajal-González, A. Ivanova, S. Dolan, C. Park, Investigation of the fate and dynamics of extracellular polymeric substances (EPS) during sludge-based photogranulation under hydrostatic conditions, Environ. Sci. Technol. 52 (2018) 10462–10471, https://doi.org/10.1021/acs.est.8b03033.

[21] APHA, Standard Methods for the Examination of Water and Wastewater, APHA, AWWA,WEF, Washington: American Public Health Association, 2012. ⟨http://www.standardmethods.org/⟩ (Accessed 27 September 2018).

[22] E. Lawrenz, E.J. Fedewa, T.L. Richardson, Extraction protocols for the quantification of phycobilins in aqueous phytoplankton extracts, J. Appl. Phycol. 23 (2011) 865–871, https://doi.org/10.1007/s10811-010-9600-0.

[23] R. Lauceri, M. Bresciani, A. Lami, G. Morabito, Chlorophyll a interference in phycocyanin and allophycocyanin spectrophotometric quantification, J. Limnol. (2017), https://doi.org/10.4081/jlimnol.2017.1691.

[24] A. Bennett, L. Bogorad, Complementary chromatic adaptation in a filamentous blue-green alga, J. Cell Biol. 58 (1973) 419–435. ⟨https://www.ncbi.nlm.nih.gov/pmc/articles/PMC2109051/⟩ (Accessed 4 January 2019).

[25] K. Sears, J.E. Alleman, J.L. Barnard, J.A. Oleszkiewicz, Density and activity characterization of activated sludge flocs, J. Environ. Eng. 132 (2006) 1235–1242, https://doi.org/10.1061/(ASCE)0733-9372(2006)132:10(1235).

[26] T. Etterer, P.A. Wilderer, Generation and properties of aerobic granular sludge, Water Sci. Technol. 43 (2001) 19–26, https://doi.org/10.2166/wst.2001.0114.

[27] G. Neale, N. Epstein, W. Nader, Creeping flow relative to permeable spheres, Chem. Eng. Sci. 28 (1973) 1865–1874, https://doi.org/10.1016/0009-2509(73)85070-5.

[28] J.H. Masliyah, M. Polikar, Terminal velocity of porous spheres, Can. J. Chem. Eng. 58 (1980) 299–302, https://doi.org/10.1002/cjce.5450580303.

[29] A.J. Mason, OpenSolver - An Open Source Add-in to Solve Linear and Integer Progammes in Excel, in: D. Klatte, H.-J. Lüthi, K. Schmedders (Eds.), Oper. Res. Proc. 2011, Springer, Berlin, Heidelberg, 2012, pp. 401–406, https://doi.org/10.1007/978-3-642-29210-1_64.

[30] J. Wu, R. Manasseh, Dynamics of dual-particles settling under gravity, Int. J. Multiph. Flow. 24 (1998) 1343–1358, https://doi.org/10.1016/S0301-9322(98)00029-9.

[31] J. Liu, P. Zhang, Y. Xiao, Z. Wang, S. Yuan, H. Tang, Interaction between dual spherical particles during settling in fluid, Phys. Fluids 33 (2021), 013312, https://doi.org/10.1063/5.0034927.

[32] A. Emadzadeh, Y.-M. Chiew, Settling velocity of porous spherical particles, J. Hydraul. Eng. 146 (2020) 04019046, https://doi.org/10.1061/(ASCE)HY.1943-7900.0001655.

[33] F. Basheer, I.H. Farooqi, Hydrodynamic properties of aerobic granules cultivated on phenol as carbon source, APCBEE Procedia 10 (2014) 126–130, https://doi.org/10.1016/j.apcbee.2014.10.029.

[34] D.J. Lee, G.W. Chen, Y.C. Liao, C.C. Hsieh, On the free-settling test for estimating activated sludge floc density, Water Res. 30 (1996) 541–550. ⟨http://www.sciencedirect.com/science/article/pii/0043135495002294⟩ (Accessed April 20, 2017).

[35] W.A.S.K. Mancell-Egala, D.J. Kinnear, K.L. Jones, H. De Clippeleir, I. Takács, S. N. Murthy, Limit of stokesian settling concentration characterizes sludge settling velocity, Water Res 90 (2016) 100–110, https://doi.org/10.1016/j.watres.2015.12.007.

[36] H.-C. Flemming, T.R. Neu, D.J. Wozniak, The EPS matrix: the "house of biofilm cells, J. Bacteriol. 189 (2007) 7945–7947, https://doi.org/10.1128/JB.00858-07.

[37] J. Wu, F.L. de los Reyes, J.J. Ducoste, Modeling cell aggregate morphology during aerobic granulation in activated sludge processes reveals the combined effect of substrate and shear, Water Res. 170 (2020), 115384, https://doi.org/10.1016/j.watres.2019.115384.

[38] J. Yang, Approaches for modeling anaerobic granule-based reactors, Bact. Biofilms (2019), https://doi.org/10.5772/intechopen.90201.

[39] W.B. Whitman, F. Rainey, P. Kämpfer, M. Trujillo, J. Chun, P. DeVos, B. Hedlund, S. Dedysh (Eds.), Bergey's Manual of Systematics of Archaea and Bacteria, first ed., Wiley, 2015 https://doi.org/10.1002/9781118960608.

[40] K. Milferstedt, W.C. Kuo-Dahab, C.S. Butler, J. Hamelin, A.S. Abouhend, K. Stauch-White, A. McNair, C. Watt, B.I. Carbajal-González, S. Dolan, C. Park, The importance of filamentous cyanobacteria in the development of oxygenic photogranules, Sci. Rep. 7 (2017) 17944, https://doi.org/10.1038/s41598-017-16614-9.

[41] H.L. Golterman, Chapter 13 Algae and their Pigments, in: Physiol. Limnol. Approach Physiol. Lake Ecosyst, Elsevier, 1975, pp. 233–247, https://doi.org/10.1016/S0167-5648(08)71070-0.

[42] N. Bj, Y. Hq, Mathematical modeling of aerobic granular sludge: a review, Biotechnol. Adv. 28 (2010) 895–909, https://doi.org/10.1016/j.biotechadv.2010.08.004.